encit 2020

ABCM
Associação Brasileira de Engenharia e Ciências Mecânicas

18th Brazilian Congress of Thermal Sciences and Engineering
November 16–20, 2020, Bento Gonçalves, RS, Brazil

ENCIT2020-0178
An In-House Finite Volume Analysis to Predict the Heat Affected Zone in TIG Welding

Stephanie Loi Brião
João Rodrigo Andrade *
Fran Sérgio Lobato
Luiz Eduardo dos Santos Paes
Louriel Vilarinho
Ruham Pablo Reis

Universidade Federal de Uberlândia, Faculty of Mechanical Engineering, Center for Research and Development of Welding Processes, Uberlândia, Minas Gerais, Brazil

stephanie.loi@ufu.br, joao.andrade@ufu.br, fslobato@ufu.br, luiz.paes@ufu.br, vilarinho@ufu.br, ruhamreis@ufu.br
* Corresponding author: joao.andrade@ufu.br

Abstract. *The Heat Affected Zone (HAZ) is considered the most relevant region of a weld bead, due to the presence of brittle phases and grain growth. By definition, the HAZ was submitted to temperatures below melting, but sufficient to cause microstructural changes. Experimentally, it is possible to identify microstructure modifications through chemical etching or measurement of hardness profile. However, there is not a criterion for HAZ boundaries based on a thermal profile resultant from the numerical simulation. Usually, the critical temperature (T_c) is adopted. For carbon steels, this temperature is* $727\ ^{\circ}C$*, where austenitization starts. The present paper proposes to consider the austenite phase fraction (f) from transformation kinetics besides this temperature, through the modified Johnson–Mehl–Avrami (JMA) equation. To investigate that, an "in-house" MATLAB-based code was developed, using the Finite Volume Method and validated experimentally for an autogenous Tungsten Inert Gas (TIG) process. The results pointed that the austenite phase fraction can be used with the critical temperature to delimit the HAZ considering the value of* 1% *of austenitization as the start value, but there is not a significant difference in practice (*0.01 *mm) when using only the critical temperature criterion. Therefore, the implementation of the JMA equation in a numerical model is more relevant to identify the regions subjected to a higher degree of phase transformation, and the consequently higher probability of brittle phases, than to delimit the HAZ boundaries.*

Keywords: *GTAW, Finite Volume, Simulation, Temperature Field, Phase Transformation*

1. Introduction

Naval (Zou *et al.*, 2020), automotive (Karakizis *et al.*, 2019), and oil industries (Sartori *et al.*, 2017) highly depend on welding processes. In the assembly stage, there is a constant need to join parts of different materials and shapes. Besides that, when problems associated to wear or cracks occur, welding processes are also used to repair (Ola *et al.*, 2019). Another range of application regards to coatings, in order to improve corrosion and abrasion resistance (Verdi *et al.*, 2017). Finally, the manufacturing of metal components has been investigated through additive manufacturing technology (Silva *et al.*, 2020).

Among the main types of welding, the Tungsten Inert Gas (TIG) procedure is given by an arc generated between a non-consumable tungsten electrode and the work-piece. Its main advantage is related to a higher quality when compared to other procedures, for example, MIG/MAG. The main reason for its good welding quality relies on the heat input, that can be controlled independently from the filler material, which results in a low defect incidence. The limitation of the TIG procedure regards the fact that it is hard to achieve higher productivity. However, recent works have shown that this drawback can be solved (Silva *et al.*, 2018), (Silva *et al.*, 2019b), (Silva *et al.*, 2019a).

A thermal analysis of welding starts at the Fusion Zone (FZ). This area is constituted by the melted material. In the Heat Affected Zone (HAZ) there are changes in the material microstructure. The farthest area from the weld is designated as Base Metal (BM) and remains unchanged (phase transformation does not happen) as a result of processing.

Among the cited regions, HAZ is the most relevant one. Brittle phases (Rafieazad *et al.*, 2019) and grain growth (Chen *et al.*, 2015) can occur, which is deleterious for material integrity. There are many definitions for this region from classical welding literature. According to O'Brien and Guzman (2007), the HAZ consists of a region near the FZ where

microstructural changes occurred and can be observed through chemical etching or measurement of hardness profile. Kou (2003) states that in HAZ peak temperatures from thermal cycles were not sufficient to cause melting but caused significant microstructural modifications. Lippold *et al.* (2015) define it as a region that, although not melted, was affected by the process heat. In addition, claims that, for carbon steels, the HAZ temperature range varies between A1 (727 °C) of Fe-C diagram, which corresponds to the lowest austenitization (critical) temperature (T_c), and the solidus temperature, which is to the maximum temperature where the alloy is solid, as shown in Fig. 1.

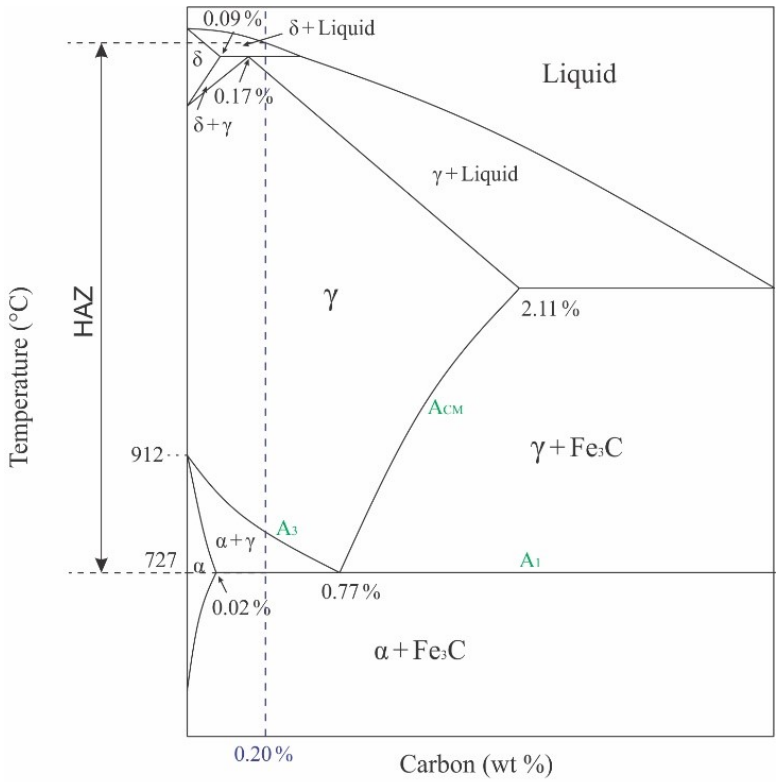

Figure 1. Schematic of Fe-C diagram showing the HAZ temperature range for a SAE 1020 carbon steel (0.20% Carbon wt %).

For low carbon steels as the SAE 1020, the microstructural change involves phase transformation of ($\alpha + Fe_3C$) to ($\alpha + \gamma$) and includes carbon solubilization from cementite to austenite, which is not instantaneous. Therefore, another requirement for phase transformation is time. The γ phase fraction (f) can be calculated with the modified Johnson–Mehl–Avrami (JMA) equation, considering transformation kinetics (Zhang *et al.*, 2002a). One input is the thermal cycle illustrated schematically in Fig. 2. After austenitization, the cooling rate is the main factor that determines the final microstructure.

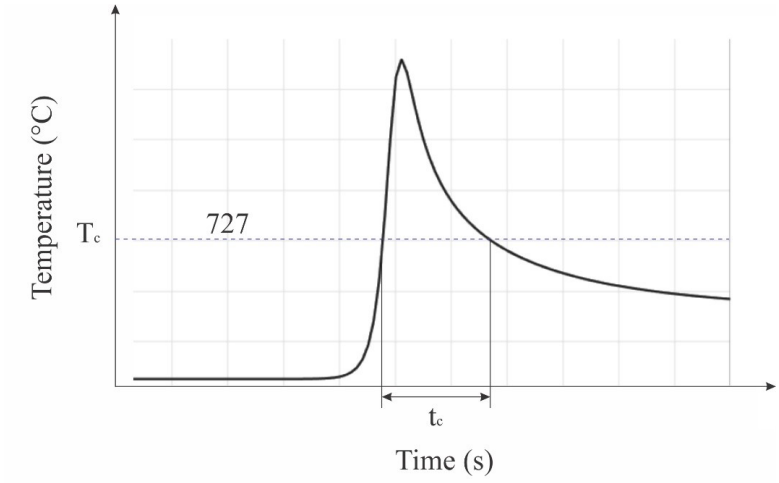

Figure 2. Schematic of thermal cycle showing critical temperature (T_c).

The classical definitions covered allow HAZ identification through experiments since involve etching and measurement of hardness profile. It is not possible to apply this methodology to determine HAZ based on computational simulation.

Numerical models are used to predict the weld thermal profile, as in Venkatkumar and Ravindran (2016) work. By means of numerical simulation, enhancement in the understanding of the main characteristics of the welding procedure can be reached. For instance, the residual stress and distortion distribution of the material structure. Also, regarding numerical simulation, inverse problems are used in order to find different parameters, such as the thermal efficiency (Magalhães *et al.*, 2018), (Magalhães *et al.*, 2015). However, in these articles, the authors do not delimit the HAZ boundary.

In the present paper, it is proposed to consider besides the critical temperature of 727 °C, the austenite fraction to delimit the HAZ. An "in-house" MATLAB-based code was developed and qualitatively validated with experimental results for the autogenous TIG process in SAE 1020 steel. This code can be adapted to allow other important analyses for welding and additive manufacturing processes.

2. Methodology

In the TIG welding process, the concentrated and high-intensity heat source has a defined moving direction. Also, the form that the heat drains is meanly by conduction in the material. Here, we assumed a point heat source, a constant speed, and a plate of rectangular dimensions with infinite thickness and parallel to its x axis the arc welding direction. Thus, the shape of the piece has length x, width y and thickness z, and the boundary conditions were applied to all surfaces. Also, the physical properties of the material depend on temperature.

2.1 Numerical model

This section presents an equations set that model the physical behavior of energy transfer in the welding process. Then, the three-dimensional heat equation herein employed is:

$$\frac{\partial H(T)}{\partial t} = \vec{\nabla} \cdot \left(k \vec{\nabla} T \right), \tag{1}$$

where T is the temperature, t is the time, k is the thermal diffusion coefficient and $\vec{\nabla}$ is the gradient vector. Additionally, the enthalpy function H considered is defined by (Crank, 1984):

$$H(T) = \int_{T_0}^{T} \left[\rho(\theta) c(\theta) + \rho(\theta) L \delta(\theta - T_m) \right] \mathrm{d}\theta, \tag{2}$$

where θ is variation of T_0 (reference temperature) and T, T_m is the melting temperature, ρ is the specific mass, c is the specific heat, L is the latent heat solidification and δ is the Dirac impulse function.

In order to solve the Eq. (1) with the Eq. (2), it was necessary to define boundary and initial conditions. Therefore, convection and radiation effects were imposed, as well as a moving heat source which describes the thermal effects of welding. The considered initial condition is $T(x, y, z, 0) = T_0 = 25$ °C, and the mathematical model for the boundary condition involving convection and radiation are given by:

$$\frac{\partial T}{\partial \xi} = \frac{h(T)(T_\infty - T)}{k(T)} + \frac{\sigma \varepsilon(T)(T_\infty^4 - T^4)}{k(T)}, \tag{3}$$

where ξ stands for the normal direction of the boundary surface, h represents the convective heat transfer coefficient, σ is the Stefan-Boltzmann constant, ε is the emissivity, and T_∞ is the room temperature.

Concerning the welding boundary condition, the heat flux, $q''(x, y, t)$, is given by a homogeneous heat surface distribution limited by a circular area with a radius R on the top surface, as detailed below:

$$q''(x, y, t) = \frac{Q(x, y, t)}{\pi R^2}, \tag{4}$$

where Q is the gross heat rate, and R is the weld radius. The region for which the welding heat flux is applied moves at a constant velocity u in x direction.

More specifically, the thermal efficiency η considered was based on the following empirical relation (Arul and Sellamuthu, 2011):

$$\eta = 71.8 + 0.006I + 0.36U, \tag{5}$$

where I and U stands for the electrical current and voltage, respectively.

Also, in Eq. (4) the welding heat source radius R was established by the equality below (Arul and Sellamuthu, 2011).

$$R = \sqrt{\frac{3.29 + 1.01 \times 10^{-2} IU - 0.04U}{\pi}}. \tag{6}$$

Thus, to find the solution in Eq. (1) the thermal energy transfer equation was discretized by means of the finite volume method. Then, this equation was integrated in time using the first-order explicit Euler method, and its diffusive term was approximated by the central difference scheme.

In addition to the critical temperature, time is an important factor for microstructure analysis in welding processes. This is due to phase transformation being not instantaneous, which means that if austenitization does not happen, new phases can not be formed and the initial microstructure will not change.

In order to quantify the microstructure change in the welding process, Krüger (1993) and Zhang *et al.* (2002b) proposed the modified Johnson–Mehl–Avrami (JMA) equation to qualitatively determine the phase transformation rates under a thermal cycle for steel:

$$f = 1 - \exp\left[-\left\{\sum_{i=1}^{m} k_0 \exp\left(-\frac{Q}{RT_i}\right)\Delta t\right\}^n\right], \tag{7}$$

where f stands for the transformed γ phase fraction after time $m\Delta t$, Q is the activation energy of the $\alpha \rightarrow \gamma$ transformation, n and k_0 are model coefficients, R is the universal gas constant, Δt the time step, T_i the temperature at ith time step, and m indicates the total number to discrete time steps. According to Zhang *et al.* (2002a), for a low carbon steel, $Q = 117.07$ kJ/mol, $n = 1.62$ and $k_0 = 1.24 \times 10^5$.

2.2 Welding simulation parameters

The simulation of the autogenous TIG welding process was performed in an "in house" MATLAB algorithm with a non-uniform mesh. A total of $328,972$ elements was applied to the simulation grid, for which the length of the most refined element is given by $\Delta l_{min} = 2.5 \times 10^{-4}$ mm. Mesh refinement was applied in the region near the heat source. Figure 3 displays the mesh used in numerical simulations whose greater refinement is in plate center. Moreover, the time step for time integration was $\Delta t = 5.0 \times 10^{-4}$ s. The numerical domain was set to have the same dimensions as the experiments. Then, an autogenous welding process was simulated on a carbon steel plate, similar to SAE 1020, with length $L_x = 250$ mm, width $L_y = 100$ mm and thickness $L_z = 6.42$ mm. Therefore, the welding source path is given by a straight line starting at $(x, y)_{init} = (0, 50)$ mm and ending at $(x, y)_{end} = (245, 50)$ mm.

In this work, the process parameters considered are given by Tab. 1. The welding power P can be calculated multiplying current I by voltage U, since both are near constant. Using the values of Tab. 1 the power was calculated and resulted in $P = 2300$ W. The initial plate temperature attributed in the simulation was $T_0 = 25$ °C. In addition, the physical properties of steel material were adopted based on Li *et al.* (2016) work. Considering the carbon steel material, its emissivity is given by $\varepsilon = 0.5$ and its melting temperature $T_m = 1538$ °C. By Tab. 1 the thermal efficiency in Eq. (5) and heat source radius in Eq. (6) are calculated, resulting in $\eta = 0.77$ and $R = 2.86$ mm, respectively.

Table 1. Welding parameters.

Welding current (I)	200 A
Welding Voltage (U)	11.5 V
Welding Speed (V_s)	15 cm/min

2.3 Validation

To validate the numerical model, an experiment was conducted with the same parameters specified in Sec. 2.2, through a multiprocess IMC Digiplus A7 welding power source. A robotic manipulator SPS Tartílope V4 was used to control the welding speed. Argon was selected as shielding gas. The tungsten electrode was doped with 2% Thorium, had a 3.2 mm diameter and 30 °C tip angle. Transversal sections were prepared using a metallographic procedure that includes sandpaper classifications of $80, 320, 400, 600$ and 1200, besides 1.0 μm alumina polishing. Nital 10% was used during 7 s to reveal HAZ.

3. Results and Discussion

The weld profile resultant from the developed code considering two methodologies for HAZ delimitations are shown in Fig. 4. In (a), the HAZ was limited using only the critical temperature T_c, with peak temperatures above 727 °C, and in (b), using the austenitization phase fraction f.

For the critical temperature criterion, the HAZ starts at 5.77 mm from the weld center line. However, austenitization reaches 1% at 5.76 mm from the weld center line and ends (99%) at 4.61 mm from the weld center line. Although the criterion usually applied considering the critical temperature is sufficient to limit the largest region where microstructure changes could occur, Zhang *et al.* (2002a) kinetics equation enables the calculation of phase transformation percentile,

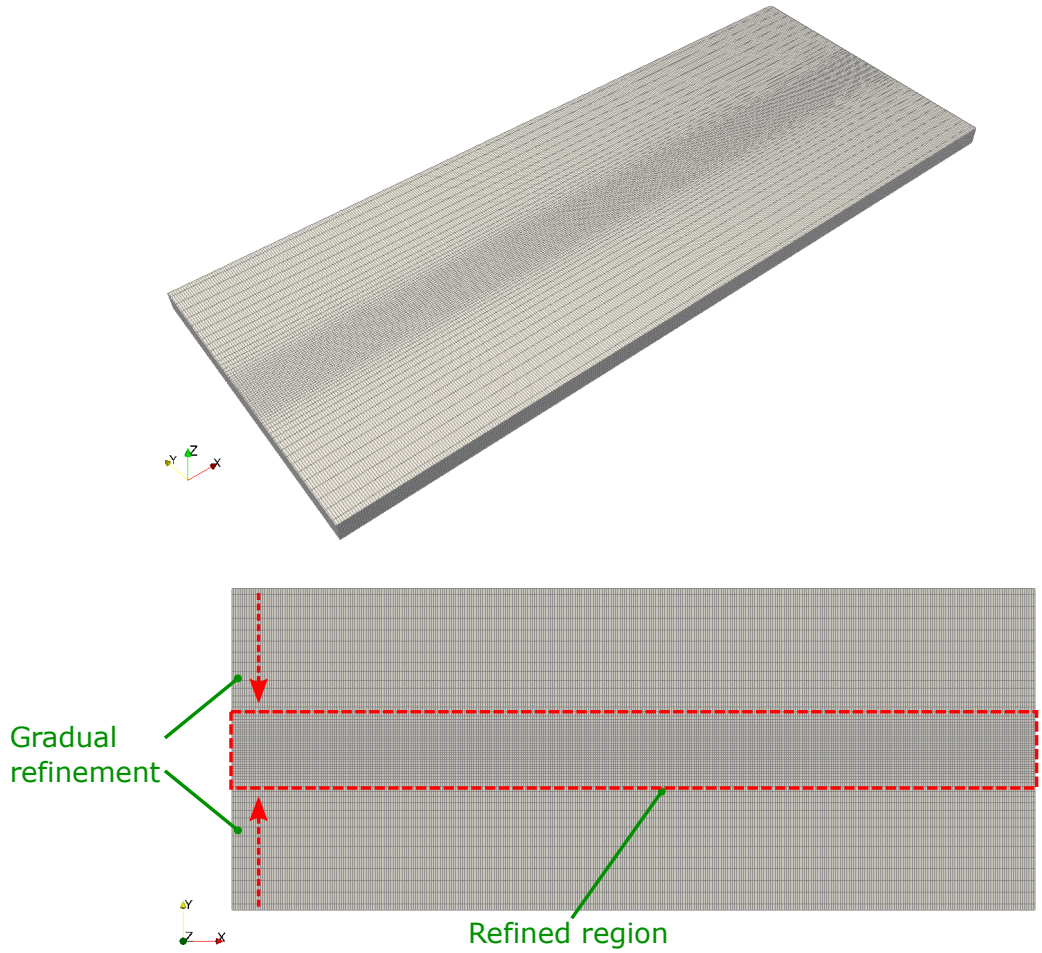

Figure 3. Mesh used in numerical simulation.

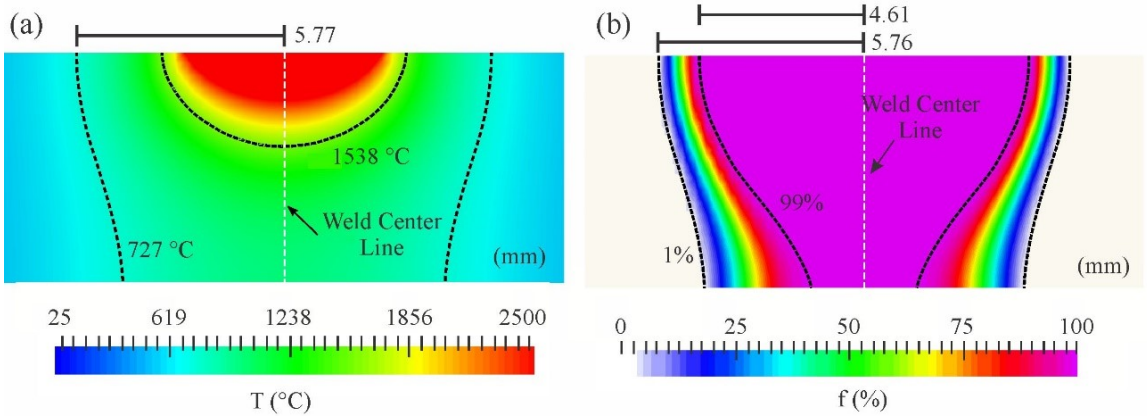

Figure 4. Simulated weld profile. (a) Temperature field. (b) Austenitization field.

and as a result, know the regions that were more affected by the heat. However, it was noted a 0.01 mm difference relative to the critical temperature criterion when the austenitization criterion was adopted, which is not relevant in practice. On the other hand, the identification of regions with a lower and higher degree of austenitization is important for welding, since if the component is subjected to a steep cooling rate between 800 °C and 500 °C, the percentile of brittle phases such as martensite is proportional to the austenite phase fraction. In this temperature range, austenite transforms to lower temperature transformation products. This can be verified in Rafieazad *et al.* (2019) work. In spite of being a low carbon alloy, martensite was formed in the HAZ. The amount of this phase was not large since steep cooling rates happened just in the $\alpha + \gamma$ region of the Fe-C diagram, where just part of the microstructure transformed to γ, originating Localized Brittle Zones (LBZ). Considering the situation were cooling rates happened in the $100\%\gamma$ region, the entire microstructure would be fragile.

The definition from O'Brien and Guzman (2007) and Lippold *et al.* (2015) cover the HAZ as a region where mi-

crostructure changes happened but do not specify a quantitative criterion for that. Kou (2003) states that the microstructure changes must be significative, but neither suggests a minimum value for phase transformation. Despite this value is not available in the literature, based on the developed code, it is possible to identify regions with a higher and lower degree of austenitization. To qualitatively validate the code, the simulated weld profile was compared with the experimental one, shown in Fig. 5.

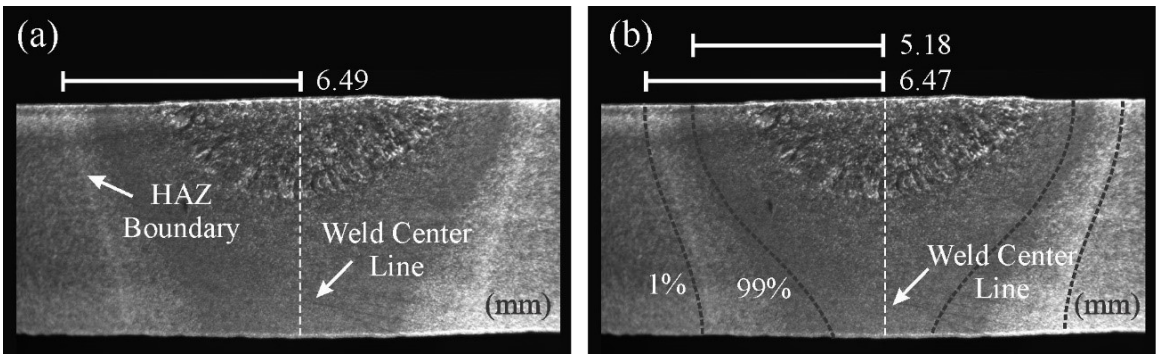

Figure 5. (a) Experimental weld profile showing the HAZ boundary relative to the weld center line. (b) Experimental weld profile showing the points where austenitization starts (1%) and ends (99%) relative to the weld center line.

In Fig. 5 (a), the HAZ starts at 6.49 mm from the weld center line. Therefore, the model can predict the HAZ boundary by 89%. Assuming this as a systematic error, the points relative to 1% of austenite phase fraction and 99% of austenite phase fraction are located at 6.47 mm and 5.18 mm from the weld center line in Fig. 5 (b), respectively.

Based on the above discussion, the austenite phase fraction can be used with the critical temperature to delimit the HAZ considering the value of 1% of austenitization as the start value, but there is not a significant difference in practice when using only the critical temperature criterion. Therefore, the implementation of the JMA equation in a numerical model is more relevant to identify the regions subjected to a higher degree of phase transformation, and the consequently higher probability of brittle phases, than to delimit the HAZ boundaries.

4. Conclusions

This paper proposed a methodology to estimate the HAZ region from the TIG process based not only on the critical temperature of 727 °C but also on the austenite phase fraction f from transformation kinetics. The following conclusions can be drawn:

- The austenite phase fraction can be used with the critical temperature to delimit the HAZ considering the value of 1% of austenitization as the start value, but there is not a significant difference in practice (0.01 mm) when using only the critical temperature criterion.

- The implementation of the JMA equation in a numerical model is more relevant to identify the regions subjected to a higher degree of phase transformation and the consequently higher probability of brittle phases than to delimit the HAZ boundaries.

- The comparison of experimental and numerical results allowed the validation of the "in-house" Finite Volume code developed. The model could predict the HAZ boundary by 89%.

5. Acknowledgements

The authors would like to acknowledge the financial technical support from the Petróleo Brasileiro S.A. (Petrobras), Agência Nacional do Petróleo (ANP) and the Brazilian funding agencies Coordenadoria de Aperfeiçoamento de Pessoal de Nível Superior (CAPES), Conselho Nacional de Desenvolvimento Científico e Tecnológico (CNPq), Fundação de Amparo à Pesquisa do Estado de Minas Gerais (FAPEMIG) and Centro para Pesquisa e Desenvolvimento de Processos de Soldagem (LAPROSOLDA).

6. References

Arul, S. and Sellamuthu, R., 2011. "Application of a simplified simulation method to the determination of arc efficiency of gas tungsten arc welding (gtaw) and experimental validation". *International Journal of Computational Materials Science and Surface Engineering*, Vol. 4, No. 3, pp. 265–280.

Chen, X., Chen, X., Xu, H. and Madigan, B., 2015. "Monte carlo simulation and experimental measurements of grain growth in the heat affected zone of 304 stainless steel during multipass welding". *The International Journal of Advanced Manufacturing Technology*, Vol. 80, No. 5-8, pp. 1197–1211.

Crank, J., 1984. *Free and Moving Boundary Problems*. Claredon Press, Oxford University Press, New York, United States.

Karakizis, P., Pantelis, D., Dragatogiannis, D., Bougiouri, V. and Charitidis, C., 2019. "Study of friction stir butt welding between thin plates of AA5754 and mild steel for automotive applications". *The International Journal of Advanced Manufacturing Technology*, Vol. 102, No. 9-12, pp. 3065–3076.

Kou, S., 2003. "Welding metallurgy". *New Jersey, USA*, pp. 431–446.

Krüger, P., 1993. "On the relation between non-isothermal and isothermal kolmogorov-johnson-mehl-avrami crystallization kinetics". *Journal of Physics and Chemistry of Solids*, Vol. 54, No. 11, pp. 1549–1555.

Li, H.X., Zhu, W.Z., Ruvalcaba, D., Mortensen, D., van der Plas, D., Fjaer, H.G. and Zhuang, L.Z., 2016. "Influence of liquid core reduction on stress-strain distribution and strand deformation in a thin slab caster". *ISIJ International*, Vol. 56, No. 9, pp. 1616–162.

Lippold, J.C. *et al.*, 2015. *Welding metallurgy and weldability*. Wiley Online Library.

Magalhães, E.d.S., de Carvalho, S.R., Silva, S.M.M.L.E. *et al.*, 2015. "The use of non-linear inverse problem and enthalpy method in gtaw process of aluminum". *International Communications in Heat and Mass Transfer*, Vol. 66, pp. 114–121.

Magalhães, E.d.S., Paes, L.E.d.S., Pereira, M., da Silveira, C.A., Pereira, A.d.S.P. and e Silva, S.M.M.L., 2018. "A thermal analysis in laser welding using inverse problems". *International Communications in Heat and Mass Transfer*, Vol. 92, pp. 112–119.

O'Brien, A. and Guzman, C., 2007. *Welding handbook: welding processes*. American Welding Society.

Ola, O., Valdez, R., Oluwasegun, K., Ojo, O., Chan, K., Birur, A. and Cuddy, J., 2019. "Process variable optimization in the cold metal transfer weld repair of aerospace ZE41A-T5 alloy using central composite design". *The International Journal of Advanced Manufacturing Technology*, Vol. 105, No. 11, pp. 4827–4835.

Rafieazad, M., Ghaffari, M., Nemani, A.V. and Nasiri, A., 2019. "Microstructural evolution and mechanical properties of a low-carbon low-alloy steel produced by wire arc additive manufacturing". *The International Journal of Advanced Manufacturing Technology*, Vol. 105, No. 5-6, pp. 2121–2134.

Sartori, F., Silva, R.H.G., Dutra, J.C., Paes, L.E.d.S., Schwedersky, M.B. and Marques, C., 2017. "Uma análise comparativa entre diferentes versões de variantes modernas do processo mig/mag para o passe de raiz em soldagem orbital". *Soldagem & Inspeção*, Vol. 22, No. 4, pp. 442–452.

Silva, L.J., Souza, D.M., de Araújo, D.B., Reis, R.P. and Scotti, A., 2020. "Concept and validation of an active cooling technique to mitigate heat accumulation in waam". *The International Journal of Advanced Manufacturing Technology*, pp. 1–11.

Silva, R.H.G., dos Santos Paes, L.E., de Sousa, G.L., Marques, C., Viviani, A.B., Schwedersky, M.B. and da Costa Pinto, T.L.F., 2019a. "Design of a wire measurement system for dynamic feeding tig welding using instantaneous angular speed". *The International Journal of Advanced Manufacturing Technology*, Vol. 101, No. 5-8, pp. 1651–1660.

Silva, R.H.G., dos Santos Paes, L.E., Marques, C., Riffel, K.C. and Schwedersky, M.B., 2019b. "Performing higher speeds with dynamic feeding gas tungsten arc welding (gtaw) for pipeline applications". *Journal of the Brazilian Society of Mechanical Sciences and Engineering*, Vol. 41, No. 1, p. 38.

Silva, R.H.G., dos Santos Paes, L.E., Okuyama, M.P., de Sousa, G.L., Viviani, A.B., Cirino, L.M. and Schwedersky, M.B., 2018. "Tig welding process with dynamic feeding: a characterization approach". *The International Journal of Advanced Manufacturing Technology*, Vol. 96, No. 9-12, pp. 4467–4475.

Venkatkumar, D. and Ravindran, D., 2016. "3d finite element simulation of temperature distribution, residual stress and distortion on 304 stainless steel plates using gta welding". *Journal of Mechanical Science and Technology*, Vol. 30, No. 1, pp. 67–76.

Verdi, D., Múnez, C., Garrido, M. and Poza, P., 2017. "Process parameter selection for inconel 625-Cr 3 C 2 laser cladded coatings". *The International Journal of Advanced Manufacturing Technology*, Vol. 92, No. 5-8, pp. 3033–3042.

Zhang, W., Elmer, J.W. and DebRoy, T., 2002a. "Kinetics of ferrite to austenite transformation during welding of 1005 steel". *Scripta Materialia*. ISSN 13596462. doi:10.1016/S1359-6462(02)00040-4.

Zhang, W., Elmer, J. and DebRoy, T., 2002b. "Modeling and real time mapping of phases during gta welding of 1005 steel". *Materials Science and Engineering: A*, Vol. 333, No. 1, pp. 320 – 335. ISSN 0921-5093. doi: https://doi.org/10.1016/S0921-5093(01)01857-3. URL `http://www.sciencedirect.com/science/article/pii/S0921509301018573`.

Zou, X., Sun, J., Matsuura, H. and Wang, C., 2020. "Unravelling microstructure evolution and grain boundary misorientation in coarse-grained heat-affected zone of EH420 shipbuilding steel subject to varied welding heat inputs". *Metallurgical and Materials Transactions A*, pp. 1–7.

7. Responsibility Notice

The authors are solely responsible for the printed material included in this paper.